

Nano-particle Study on Non-thermal Plasma Exhaust from Waste Cooking Oil Biodiesel Combustion through Optical and Scanning Mobility Sizers

Sarapon Thitipatanapong¹, Sathaporn Chuepeng² and Poranat Visuwan^{1,2*}

¹ Department of Mechanical Engineering, Faculty of Engineering, Kasetsart University

² ATAE Research Unit, Department of Mechanical Engineering, Faculty of Engineering at Sriracha, Kasetsart University Sriracha Campus

* Corresponding author, E-mail: poranat@eng.src.ku.ac.th

Received: 28 November 2021; Revised: 9 December 2021; Accepted: 24 December 2021

Online Published: 17 March 2022

Abstract: Ascending usage of alternative fuel is primarily due to the fossil fuel predicament. A campaign for renewable energy to upsurge biofuel from wasted oil is progressively addressed. This has encouraged biodiesel to be applied for agricultural and transport sectors as a diesel fuel substitution. Diesel engines are favorable in fuel efficiency that relates to a reduction of greenhouse gas emissions. Typically, diesel combustion products are a concern for nitrogen oxides inversion of particulate matter. Nevertheless, non-thermal plasma (NTP) is a technique that can mitigate these emissions and may affect to particulate matter characterization. This paper demonstrates a study on the particulate matter-related emissions under NTP state of a four-cylinder diesel engine fueled with waste cooking oil biodiesel (WCO) in comparison to regular diesel. An optical and scanning mobility sizers were used to analyze the particle number and its related characteristics. Basically, the total particle number and surface area concentrations were higher for WCO at the smaller size, leading to the lesser total particle mass. When NTP charger was equipped, the particle masses were reduced for both fuels as caused by electrostatic phenomena that combine small particles to a larger size with lesser concentration. A greater extent of particle coagulation for regular diesel was observed. The NTP charger simultaneously reduced particulate matter and nitric oxide emissions.

Keywords: biodiesel; diesel; emission; non-thermal plasma; particulate matter; waste cooking oil



1. Introduction

Biodiesel fuels in the forms of fatty acid ethyl ester (FAEE) or fatty acid methyl ester (FAME) are mainly derived from various sources of agricultural materials [1]. Different biodiesel generations are dependent on their source. The first biodiesel generation is principally from animal fats and vegetable oils [2]. Nowadays and later, a more rigid regulation in food waste management is becoming enforcement [3]. Therefore, waste cooking oil (WCO) used as a raw material for producing biodiesel can mitigate food waste issues in several countries. WCO based biodiesel exhibits potentiality in reducing some regulated emissions from diesel engines [4]. However, complicated production processes and compliance to biodiesel standards for road diesel vehicles must be in consideration [5]. WCO biodiesel can be homogeneously mixed with ordinary fossil diesel fuel and can be used in present diesel engines depending on their generations and calibration [6]. Nevertheless, nitrogen oxides (NO_x) emission may increase and negative effects on human health and the environment are foreseeable [7].

Non-thermal plasma (NTP) is an effective technique to lessen diesel engine emissions [8]. In non-equilibrium thermodynamics, NTP is associated with the electrostatic field. NTP is frequently used in implementation that is related

to particulate matter (PM) and soot [9]. The plasma field is created by electrical discharge electrode poles which are partitioned by a dielectric barrier discharge (DBD) [10]. Applying an NTP reactor for a diesel after-treatment system can lower the PM by low-temperature oxidation [11].

Moreover, an NTP with dielectric barrier discharge lowered NO_x emissions by producing non-thermal equilibrium plasma to the simulated exhaust gas [12]. The NTP with 27 J/L energy density can reduce NO_x and soot from real diesel exhaust gas [13]. A dielectric barrier discharge with 1485 J/L specific input energy of the pulsed power generator can achieve a maximum of 46% NO_x reduction for diesel engines [14]. Additionally, the NTP equipped with a selective catalytic reduction (SCR) can reduce the NO_x from the diesel exhaust gas by the low-temperature oxidation at room temperature [15]. The amalgamated techniques of NTP and adsorption-base technique accelerated the NO_x removal by altering nitric oxide (NO) to nitrogen dioxide (NO_2) more than 95% [16]. The thermogravimetric analysis (TGA) proclaimed the decrease of soluble organic fraction (SOF) after NTP treated by 21.7%. The structural characteristics of diesel PM with an NTP device were explained by a scanning electron microscope (SEM). The diameter of PM was smaller, and the agglomeration degree was lessened [17].



From the literature reviewed, there have been various studies including NTP system improvements for diesel emissions. Nevertheless, there are insufficient number of knowledges that take a specific approach towards the effect of NTP charger on renewable fuel from waste product. Additionally, no studies have been carried out on the research of WCO fuels on NTP charger performance.

The objective of this study is to characterize the PM from a multi-cylinder diesel engine with exhaust NTP operated on WCO. The experiment was also commissioned by regular Diesel fuel without engine re-calibration. The PM is characterized by a scanning mobility particle sizer (SMPS) incorporated with an optical particle sizer (OPS). Particle number, surface area, and mass concentration - size distributions will be analyzed and discussed.

2. Materials and Method

2.1 Particle Source

The experimental study was conducted on a water-cooled diesel engine with a pump-line-nozzle fuel injection system. Main engine specifications are listed in Table 1.

2.2 Test Cell Apparatus

The engine was loaded by a 200-HP eddy-current Dynamite dynamometer (Model 012-200-1K). Air mass flow rate was measured using Testo (Model 435) with $\pm 0.3\%$ accuracy. Fuel mass flow rate was measured using CST

electronic balance (Model CDR-3) with ± 0.05 g accuracy over a specified time. Engine operating parameters e.g., local temperatures were obtained by the National Instrument data acquisition system (Model USB-6218) with LabVIEW-based application. The experimental diagram for the test cell apparatus is depicted in Fig. 1.

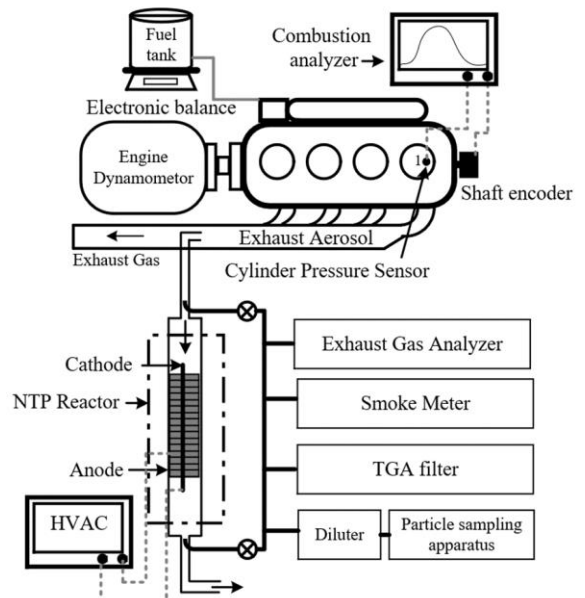


Fig. 1 Experimental diagram

Table 1 Engine specifications

Engine	Specifications
Type	Four-cylinder, in-line
Fuel system	Direct injection
Bore	91.1 mm
Stroke	95.0 mm
Displacement	2476 cc
Maximum torque	142 Nm at 2500 rpm
Maximum power	55 kW at 4200 rpm
Compression ratio	21:1



2.3 NTP Configuration

The NTP system was made up of a high voltage (25 kV) transformer with a 15 kHz discharge frequency. The input power of the NTP system is 67.3 Watts. The NTP discharge power is 59.2 Watts. The consumed energy during the discharge procedure was calculated from the voltage and current output. The specific energy density (SED) of NTP device is fixed at 50.55 J/L by controlling the exhaust gas flow at a constant rate. NTP charger's anode was coiled around a dielectric barrier with 50 mm diameter and 300 mm length. With typical charging, the NTP charger was supplied by a regular 12-VDC battery. The NTP charger was positioned approx. 3 m from exhaust valves. At the NTP charger inlet, the exhaust gases were kept at 200 °C temperature to reproduce actual engine usage in daily life applications. After the exhaust gas flowed passing through the NTP, the temperature of treated exhaust gas dropped down to 183 °C in all of the tested conditions.

2.4 Test Fuel

The fuels used in the test were waste cooking oil biodiesel (WCO) and regular 5% palm-oil-based biodiesel blended diesel (Diesel). Their main properties are shown in Table 2.

2.5 Operating condition

The engine was operated at a constant speed of 1500 rpm while the engine load used in this

study is 4 bars on the brake mean effective pressure (BMEP) scale. The fuel was controlled to the set temperature of 40 ± 1 °C to avoid PM mis-interpretation. The engine was tested without the use of exhaust gas recirculation (EGR). The speed is chosen by the frequent use of the loaded application, and it is nearby the maximum torque occurrence produced by the engine. Furthermore, the engine load at 4 bar BMEP is simulated for regular use in real engine operating conditions.

2.6 Exhaust Gas and Smoke Measurements

Nitric oxide (NO) emission from the engine was measured by a Horiba exhaust gas analyzer (Model MEXA-584L). This gas analyzer is based on the non-dispersive infrared (NDIR) technique. The NDIR technique measures the wavelength absorption of targeted gas in the infrared spectrum to identify certain gases. The gas analyzer was accurately measured by 4% reading in the range of 0-4000 ppm, 0-10 %vol., 0-20 %vol. and 0-10000 ppm for NO, CO, CO₂ and HC, respectively which can be converted to g/kWh by calculation.

Table 2 Test fuel properties

Analysis	Diesel	WCO
Flash point (°C)	70	143
Density (g/cm ³)	0.81	0.86
LHV (MJ/kg)	45.2	39.9
Water content (ppm)	77.5	1060.7
Cetane Index	50.9	55.5
Oxidation stability at 110 °C (h)	30.88	6.85



A Motorscan smoke meter (Model 9010) measured the exhaust gas opacity percentage and the calculated PM in g/kWh can be determined. The measurement range, uncertainty and accuracy of exhaust gas and smoke are shown in Table 3.

2.7 PM Size Distribution Determination

The measurement of PM number concentration in comparison between with- and without-NTP charger conditions was based on a partial flow. By iso-kinetically drawing into a 10:1 diluter, the sampled gas was diluted by oxygen (Praxair, 99.7% purity). The diluted samples were drawn to a TSI optical particle sizer (Model OPS 3330) and a TSI scanning mobility particle sizer (Model NanoScan SMPS 3910). The SMPS and OPS can measure PM in the ranges of 10 to 400 nm and 300 to 10,000 nm, respectively. Exhaust gas samples in each condition were collected for 30 seconds after

stabilization. The particle number concentrations after the dilution was already corrected and are shown here as typical exhaust gas emissions.

2.8 Thermogravimetric Analysis

To prepare for thermogravimetric analysis (TGA), the PM specimens of exhaust gas were sniffed through uncoated microfiber filter papers (Whatman, Model GF/C) at a constant volume flow rate. To prevent volatile material evaporation after collection, the samples were stored in a cooler under secured vessels. PM samples from the engine were investigated by a thermogravimetric analyzer (Perkin Elmer, Model Pyris 1 TGA) to estimate for their compositions. The analyzer was at 2°C precision, 0.1 µg sensitivity and 0.02% accuracy of the balance. The samples were treated according to the heating program shown in Table 4.

Table 3 Measurement accuracy and uncertainty

Measurand	Specification		
	Measuring range	Accuracy	Uncertainty
CO	0-10 %vol	±1.7%	±1.7%
CO ₂	0-20 %vol	±1.7%	±1.7%
HC	0-10000 ppm-vol	±4%	±4%
NO	0-4000 ppm-vol	±1.7%	±1.7%
Smoke opacity	0-100	±2%	±2%
Temperature measurement	-40 to 1100 °C	±1 °C	±0.72%
Air mass flow	0 to 20 m/s	±0.3%	±0.3%
Fuel mass flow	0 to 2000 g	±0.05 g	±0.05%

**Table 4** Heating program for TGA

Step	Heating program
1	Constant ambient temperature in N ₂ for 10 min
2	Ramping for the rate of 15°C/min in N ₂ to 550°C
3	Constant temperature of 550°C in N ₂ for 15 min
4	Constant temperature in air for 15 min
5	Reducing temperature to 250°C in N ₂

2.9 Calculation Parameters

The particle mean diameters can be determined in three substantial categories [18], count mean diameter (CMD), area mean diameter (AMD) and mass mean diameter (MMD). Those were defined and calculated by Eq. (1) – (3).

$$\text{CMD} = \frac{\sum_1^u nD_p}{N} \quad (1)$$

$$\text{AMD} = \frac{\sum_1^u aD_p}{A} \quad (2)$$

$$\text{MMD} = \frac{\sum_1^u mD_p}{M} \quad (3)$$

Where n is number concentration, a is area concentration, m is mass concentration and D_p is equivalent diameter. The number concentration (n) can be directly obtained by the measurement. l and u are the minimum and maximum particle sizes, respectively. Meanwhile, the N , A , and M are total concentrations of number, area, and mass, respectively.

The specific energy density (SED) is defined as the ratio of the discharge power of the NTP generator (W) to the diesel exhaust gas flow rate (L/min) that can be calculated by Eq. (4).

$$\text{SED} = \frac{\text{NTP discharge power}}{\text{gas flow rate}} \times 60 \quad (4)$$

2.10 Measurement Uncertainty

The uncertainty from the measurement can occur during the experiment as affected by device calibration, ambient temperature, apparatus status, and test procedures. Emission and engine parameter measurements were repeated three times, and the average values were recorded. The arithmetic mean is used to calculate the uncertainty in this experiment. The measurement accuracy and uncertainty of the experiment are displayed in Table 3.

3. Results and Discussion

Fig. 2 shows the distribution of particle number concentration over the range of particle diameter from WCO and Diesel combustions at 1500 rpm, 4 bar BMEP load. Unrelatedly for both fuels, the number concentrations were normally distributed over the range of particle diameter in both logarithmic scales. WCO particles gave a greater concentration in the smaller size of particle diameter while the Diesel particles gave a greater concentration in the accumulation mode (particle diameter larger than 50 nm). When



exhaust gas passed through NTP device, the maximum number concentrations were reduced around 69% and 50% for Diesel and WCO, respectively. WCO can reduce the number of concentrations because the oxygen content in biodiesel can improve combustion, while biodiesel content decreases the diesel aromatics, which are soot precursors. Thus, the results show the minor particle diameter release from WCO fueled engine [19]. In this study, the number of concentrations from WCO exhaust gas was higher than from Diesel fuel. These results can occur from the engine test condition and engine injection system [20-21]. Thus, the mass of PM from WCO is lower than Diesel fuel [22], later discussed in the next sub-topics.

Fig. 3 shows the plots of the total particle number concentration versus count mean diameter (CMD); both were calculated based on the schemes described in [18]. The total particle number concentrations were higher for WCO at a smaller size compared to Diesel. The total particle number concentrations for WCO and Diesel fuels of both stages were in the ranges of 3.28×10^6 to $5.14 \times 10^7 \text{ m}^{-3}$ and 1.38×10^7 to $4.84 \times 10^7 \text{ m}^{-3}$, respectively. The CMD for WCO and Diesel fuels were in the ranges of 50 to 60 nm and 57 to 72 nm, respectively. When NTP was equipped, the amounts of total number concentration were reduced by 21 to 46% and the CMD values were larger by 17 to 20%.

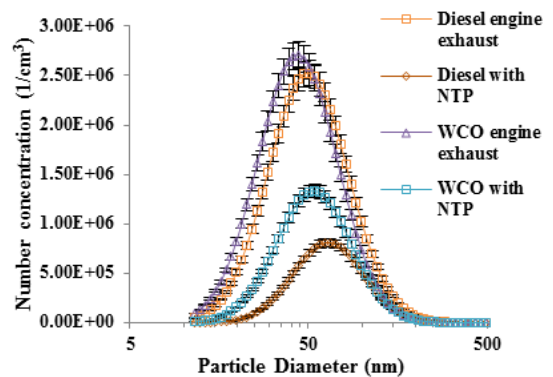


Fig. 2 Particle number size distribution at 4 bar BMEP load and 1500 rpm engine speed

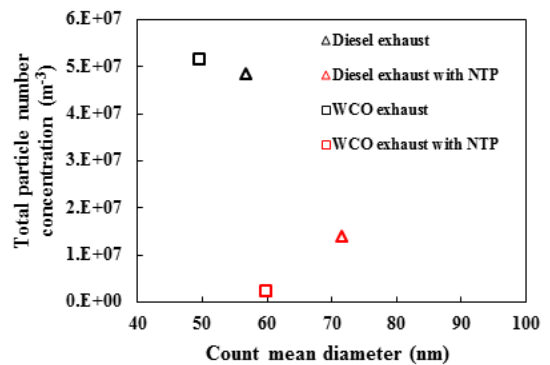


Fig. 3 Total particle number concentration versus count mean diameter

Fig. 4 depicts the distributions of particle surface area concentration over the range of particle diameter from WCO and Diesel combustions at 1500 rpm, 4 bar BMEP load. Without NTP charger activated, WCO particles show a lesser surface area in the smaller size while the Diesel particles area shows a greater surface area concentration in the larger size. When exhaust gas passed through NTP charger,



the maximum particle area concentrations were reduced approx. 52% and 31% for Diesel and WCO, respectively.

Fig. 5 depicts the plots of the total particle surface area concentration over the range of area mean diameter (AMD); both values were calculated as explained in [18]. The total particle area concentrations were higher for Diesel at a bigger size. The total particle area concentrations of both stages for WCO and Diesel were in the ranges of 2.89×10^{-4} to $4.74 \times 10^{-4} \text{ m}^{-1}$ and 2.24×10^{-4} to $5.47 \times 10^{-4} \text{ m}^{-1}$, respectively. The AMD values for WCO and Diesel fuels were in the ranges of 78 to 86 nm and 86 to 101 nm, respectively. When NTP was equipped, the amounts of total particle area concentrations were reduced by 39 to 55% while the CMD values were larger by 8 to 14%.

Fig. 6 illustrates the distribution of particle mass concentration over the range of particle diameter from WCO and Diesel combustions at 1500 rpm, 4 bar BMEP load. As a result of the numbers, WCO particles show a lesser concentration in smaller particle diameter while the diesel particles mass shows a greater concentration in the larger particle diameter. When the exhaust gas passed through NTP charger, the maximum particle mass concentrations were reduced by 47% and 23% for Diesel and WCO, respectively.

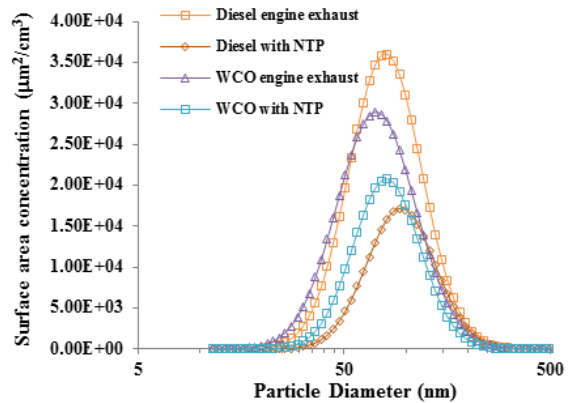


Fig. 4 Particle area size distribution at 4 bar BMEP load and 1500 rpm engine speed

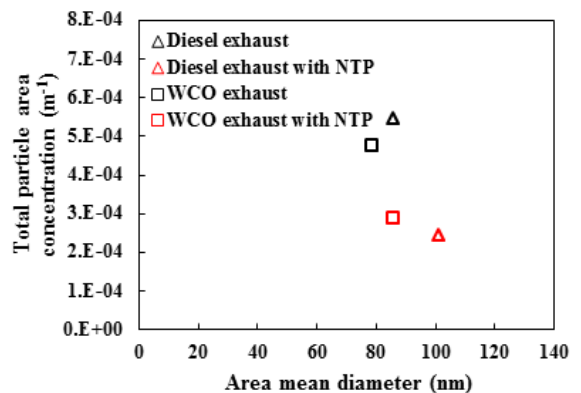


Fig. 5 Total area concentration versus area mean diameter

Fig. 7 illustrates the plots of total particle mass concentrations over the range of mass mean diameter (MMD); both values were calculated following the scheme shown in [18]. The total particle mass concentration was higher for Diesel. The total particle mass concentrations for WCO and Diesel fuels of both stages were in the ranges of 3.70×10^{-9} to $5.52 \times 10^{-9} \text{ kgm}^{-3}$ and



3.81×10^{-9} to 7.03×10^{-9} kgm^{-3} , respectively. The MMD values for WCO and Diesel fuels were in the ranges of 91 to 96 nm and 97 to 113 nm, respectively. When NTP was equipped, the amounts of total mass concentrations were reduced by 32% to 45%.

Fig. 8 shows smoke opacity of the exhaust gas with and without NTP charger equipped. The use of WCO as a fuel resulted in decreasing smoke opacity. As an oxygenated fuel of WCO, it is expected that the oxygen content will enhance the soot oxidation leading to lower smoke opacity [23-24]. Similarly, NTP can remove the PM mass which is proportional to black smoke reduction.

Fig. 9 demonstrates the PM and NO emissions with and without NTP charger equipped. The use of WCO as a fuel resulted in the increasing NO emission. The PM masses in the exhaust gases after passing through the NTP charger for all fuels were reduced. The PM reductions were by 12.9% and 16.4% for Diesel and WCO, respectively. The NO concentrations were also reduced by 28.1% and 24.6% for Diesel and WCO, respectively.

An observable escalation of the CO concentration shown in Fig. 10 for Diesel exhaust gas treated in NTP charger correlates to the reduction of the CO_2 concentration by chemical isolation. These results in reverse relation between CO and CO_2 are shown in Figs. 10 and 11, respectively.

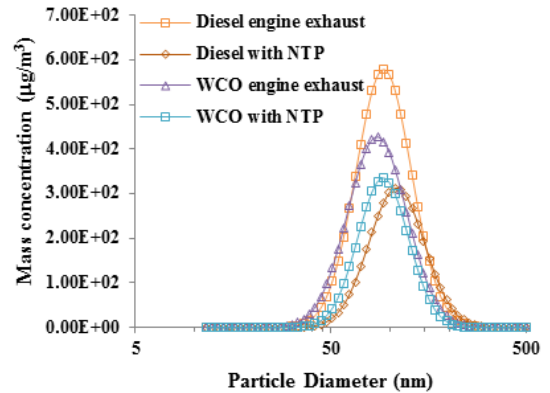


Fig. 6 Particle mass size distribution at 4 bar BMEP load and 1500 rpm engine speed

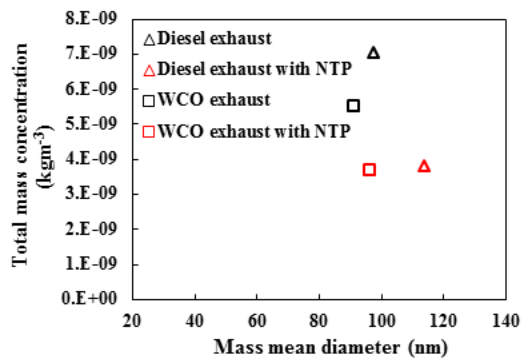


Fig. 7 Total mass concentration versus mass mean diameter

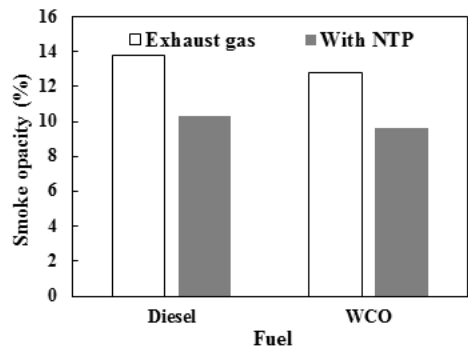
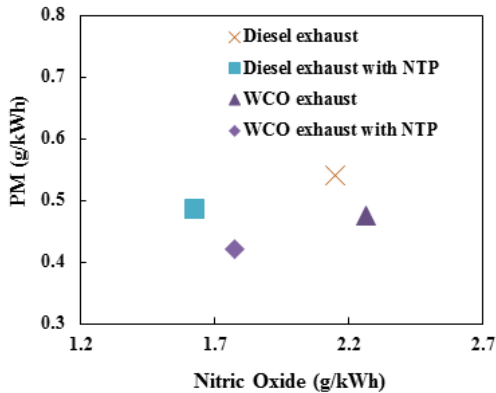
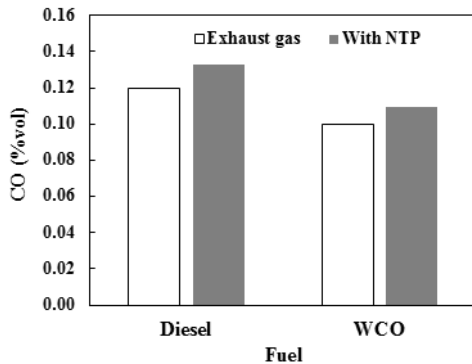
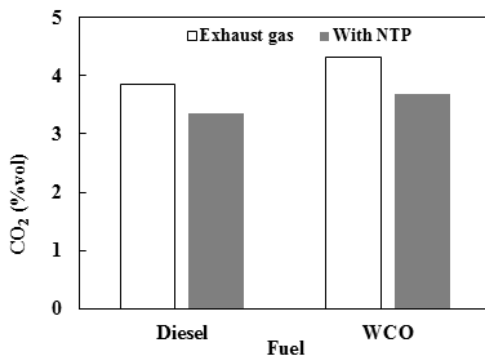


Fig. 8 Smoke opacity



บทความวิจัย

**Fig. 9** Nitric oxide and particulate matter emissions**Fig. 10** Carbon monoxide concentration**Fig. 11** Carbon dioxide concentration

Nevertheless, regarding that the CO formation to CO₂ is caused by chemical separation, the results presented a tangible difference in quantity in the rise of the CO concentration compared to the reduction of the CO₂ concentration. The production of CO₃ during CO₂ + O and CO₂ + O₃ was the believable process reaction pathway for NTP discharge that employed CO₂ as a reactant [25]. In this research, the moderately high SED value led to a small duration of the exhaust gas or particle residence time in the NTP reactor, which emerged in the PM partial oxidation [26], concerning the oxidation behavior of PM treated by the NTP reactor [27]. Therefore, an increase in CO concentration was witnessed, while the CO₂ concentration reduced as a result.

The HC concentration changes were observed and are shown in Fig. 12. The NTP charger can increase the amount of HC for both fuels. This was essentially due to the synergy among O radicals, excited electrons, and VOCs, that caused the itemization of large HC fragments into smaller HCs in a higher number, hence the greater HC concentration [28]. In this investigation, due to restrictions of the apparatus applied for HC determination (in the equivalent value of C₆H₁₄), the measurement system can only be considered that large HCs molecules, for example butane (C₄H₁₀), benzene (C₆H₆), toluene (C₇H₈), or dodecane (C₁₂H₂₆), separated into smaller and detectable HCs [29].

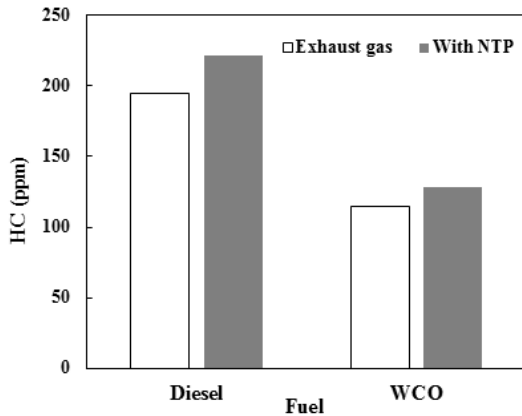


Fig. 12 Total unburned hydrocarbon concentration

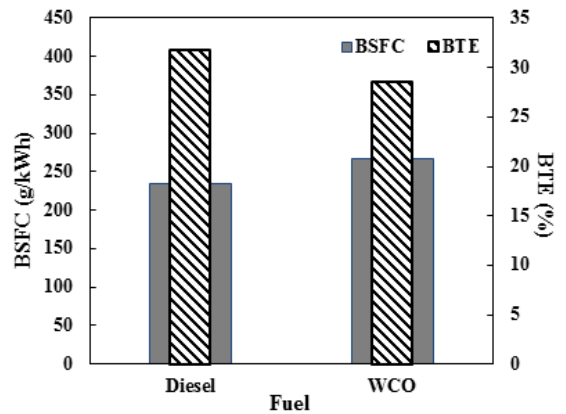


Fig. 13 Brake thermal efficiency and brake specific fuel consumption

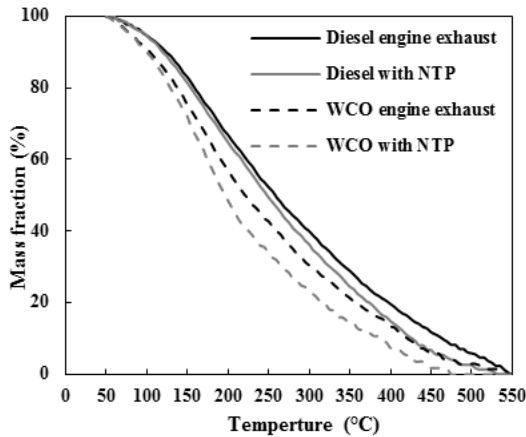
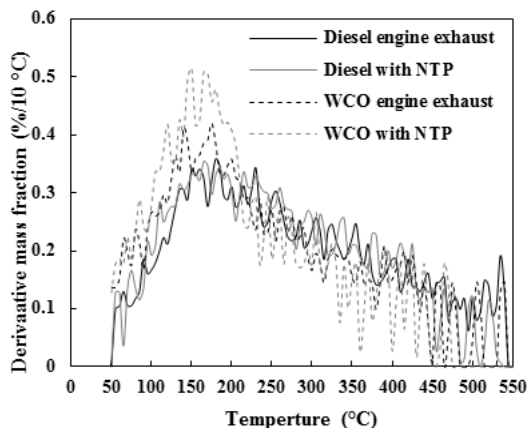
Fig. 13 presents the brake thermal efficiency (BTE) and brake specific fuel consumption (BSFC) at 4 bar BMEP load for Diesel and WCO fuels. In common, the BSFC reduced with raising engine load. Mutually, the brake power output shows an eminent effect rather than fuel consumption. When WCO was fueled, the BSFC rose higher than Diesel fuel under the same condition. It was founded that when compared with Diesel fuel, the rate of BSFC was rising by 12% for WCO, at 4 bar BMEP. These events were essentially happened by which the reduction of the heating value of WCO. The fuel mass of WCO was, therefore, increased to sustain the set load. The BSFC values are inversely affected by the BTE. The BTE is defined by the actual engine brake work divided by the fuel energy input to the engine. The BTE from the experiment was 31.7%

and 28.5% for Diesel and WCO, respectively, at 4 bar BMEP. When the engine was running in the same conditions, the BTE values of WCO fuel were lower than Diesel fuel. The reason was previously given as WCO has a lower heating value, higher density, and viscosity than Diesel fuel. The higher viscosity of the fuel leads to reduced fuel atomization, resulting in a lower value of BTE of biodiesel [19].

TGA is typically used to estimate the thermal stability of different types of substances. The weight loss of PM specimens is represented in the form of particle mass fraction that may decrease depending on their characteristics when the specimens are heated. Fig. 14 shows the weight losses of PM samples expressed in terms of the mass fraction that was reduced across TGA while the derivative mass fraction is shown in Fig. 15.



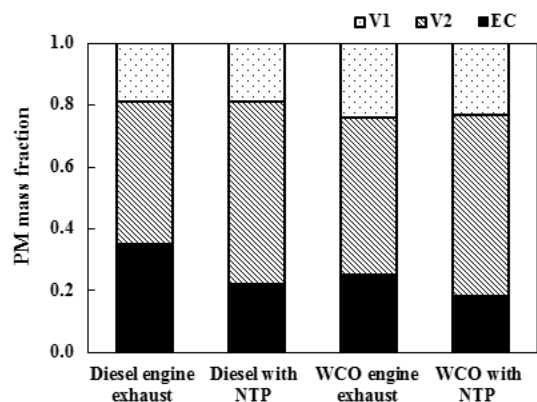
บทความวิจัย

**Fig. 14** PM weight loss at 4 bar BMEP**Fig. 15** Derivative mass fraction at 4 bar BMEP

In contrast, different fuels brought about a dissimilar PM component at engine exhaust and NTP conditions. The mass loss curves for each mode decreased at around 50-550°C under a nitrogen environment, mainly caused by the volatile substance loss and non-volatile substance oxidation. In addition, the residual mass after this process is elemental carbon. This can be explained that the PM of biodiesel includes

unburned oxygenated hydrocarbon; acceleration of the oxidation process was achieved. Moreover, after passing through NTP, the PM mass fraction was even significantly reduced compared to that of the engine exhaust condition.

Fig. 16 shows the PM mass fraction for all fuels. While heating, the specimens following the given temperature ramp program, volatile materials, or organic carbon (OC) were founded in the temperature range of 50°C to 550°C but divided into two temperature ranges. The volatile material V1, was attained in the range of 50°C to 200°C, where moisture was vaporized during the volatile material. The volatile material V2 was in the temperature range of 200°C to 550°C, where unburned hydrocarbons were oxidized. Finally, the solid elemental carbon (EC) was ranged in a temperature higher than 550°C. Therefore, the temperatures below 550°C, weight loss from devolatilization and vaporization can be founded,

**Fig. 16** PM mass fraction at 4 bar BMEP



while beyond 550°C, weight loss was caused by combustion. For all fuels, the OC amount at the exhaust gas was founded to increase when using WCO. The obtained results have resembled information reported in the literature based on other biodiesel types and test conditions [30].

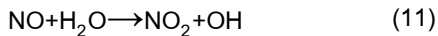
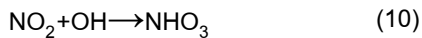
The NO reduction can be further explained by the plasma chemistry reactions through the dissociation of NO and NO₂ [31].



In an oxidizing condition of diesel exhaust gas, NO can also be converted into N₂ [32].

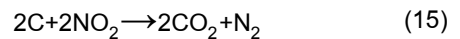


On top of that, in the presence of water, some other reactions are also contributed to NO conversion [33-34].



The results from TGA and previous research work [35] show that the NTP can reduce the elemental carbon (EC) from the exhaust gas of diesel engine operated with WCO and Diesel fuels at low and medium loads. In addition, the great reduction performance for the small size of particles can confirm that the NTP can create

low-temperature oxidation of PM [36-37]. The NO reduction can be further clarified in conjunction with the decreasing carbonaceous PM in plasma-treated gas by incineration of NO₂ according to the following reactions [38-39].



Therefore, PM and NO can be simultaneously decreased when the exhaust gas passed through the NTP device.

The results from particle size in accumulation mode show the reduction in performance of NTP. This situation has occurred by which VOF cannot well oxidize at low temperature. From the particle concentration results, the agglomeration of the nucleation mode particle to the accumulation mode particle occurred. This situation can be explained that the small particles passed through the electrostatic force and formed into the larger particle [9, 11]. This phenomenon can reduce the performance of NTP in the range of accumulation mode particles.

In terms of energy and efficiency, NTP can reduce the total mass of PM by consuming power by 67.3 Watts. The consumed power of NTP is accounted for 0.38% of engine output power. In addition, the PM removal effectiveness of this



NTP charger is the ratio of mass removed by NTP and NTP power input. The removal effectiveness values were by 9.09 and 7.63 g/kWh for Diesel and WCO, respectively. By this aspect, the NTP charger is favorable in effectiveness for Diesel fuel exhaust gas.

4. Conclusion

This work analyzes the PM number, surface area, and mass characterizations and related emissions in the four-cylinder diesel engine running on WCO with Diesel fuel in comparison. The experiment was tested on medium loads of 4 bar BMEP, 1500 rpm, with and without the use of NTP charger. The conclusions are as follows.

The NTP charger system exhibited a notable decrease in PM number and mass by generating free radicals. The synergistic outcome of PM oxidation by radical varieties and electrostatic agglomeration on PM loss have been seen in this research. The TGA results revealed a significant change in the VOCs and EC fractions as well as oxidation characteristics. Meanwhile, the gas composition analysis indicated the generation of free radicals by the NTP reactor system obliquely through consideration of the forms of the NO, CO, CO₂, and HC concentrations.

For particle number, the distributions for WCO are normally distributed in logarithmic scale form. The concentration in any size range is proportional, with the consistent particle types

referred to as nucleation and accumulation modes. The total particle number concentrations were higher for WCO at the smaller size. The particle surface area concentration distributions have corresponded to the particle number concentrations. This brings about the lesser total particle surface areas and masses for WCO fuel at the smaller size.

When NTP charger was equipped, the PM masses were reduced by 25 and 30% for WCO and Diesel, respectively in the accumulation mode. The reduction in CMD was caused by electrostatic phenomena that combine small particles to the larger size, considered as coagulation.

The NTP charger simultaneously reduced the mass of WCO's PM and NO emissions by 16.4% and 24.6%, respectively. This advocates the NTP technique that can simultaneously mitigate the trade-off emissions. Optimization of operating parameters of NTP charger for an advanced turbocharged common rail diesel engine should be prepared for future work to cope with stringent legislation.

5. Acknowledgement

Thailand Research Fund and Saveplus Limited Partnership through the Research and Researcher for Industry Project (Grant No.: PHD5710077) are acknowledged for financial support to this project.



6. References

- [1] S.J. Malode, K.K. Prabhu, R.J. Mascarenhas, N.P. Shetti and T.M. Aminabhavi, Recent advances and viability in biofuel production, *Energy Conversion and Management: X*, 2021, 10, 100070.
- [2] M. Mofijur, Sk.Y.A. Siddiki, Md. B.A. Shuvho, F. Djavanroodi, I.M.R. Fattah, H. C. Ong, M.A. Chowdhury and T.M.I. Mahlia, Effect of nanocatalysts on the transesterification reaction of first, second and third generation biodiesel sources- A mini-review, *Chemosphere*, 2021, 270, 128642.
- [3] G.G. Karunasena, J. Ananda and D. Pearson, Generational differences in food management skills and their impact on food waste in households, *Resources, Conservation and Recycling*, 2021, 175, 105890.
- [4] M. Elkelawy, E.A. Shenawy, S.K. Almonem, M.H. Nasef, H.N Panchal, H.A. Bastawissi, K.K. Sadasivuni, A.K. Choudhary, D. Sharma and M. Khalid, Experimental study on combustion, performance, and emission behaviours of diesel /WCO biodiesel/Cyclohexane blends in DI-CI engine, *Process Safety and Environmental Protection*, 2021, 149, 684-697.
- [5] C. Komintarachat and S. Chuepeng, Catalytic enhancement of calcium oxide from green mussel shell by potassium chloride impregnation for waste cooking oil-based biodiesel production, *Bioresource Technology Reports*, 2020, 12, 100589.
- [6] H. Sanli, M. Canakci, E. Alptekin, A. Turkcan and A.N. Ozsezen, Effects of waste frying oil based methyl and ethyl ester biodiesel fuels on the performance, combustion and emission characteristics of a DI diesel engine, *Fuel*, 2015, 159, 179-187.
- [7] T. Boningari and P.G. Smirniotis, Impact of nitrogen oxides on the environment and human health: Mn-based materials for the NOx abatement, *Current Opinion in Chemical Engineering*, 2016, 13, 133-141.
- [8] G.T. Kim, B.H. Seo, W.J. Lee, J. Park, M.K. Kim and S.M. Lee, Effects of applying non-thermal plasma on combustion stability and emissions of NOx and CO in a model gas turbine combustor, *Fuel*, 2017, 194, 321-328.
- [9] V. Thonglek and T. Kiatsiroat, Agglomeration of sub-micron particles by a non-thermal plasma electrostatic precipitator, *Journal of Electrostatics*, 2014, 72, 33-38.



- [10] H. Matsuno, N. Hishinuma, K. Hirose, K. Kasagi, F. Takemoto, Y. Aiura and T. Igarashi, Dielectric Barrier Discharge Lamp, United States Patent, 1998, 5757132.
- [11] C. Ma, J. Gao, L. Zhong and S. Xing, Experimental investigation of the oxidation behavior and thermal kinetics of diesel particulate matter with non-thermal plasma, Applied Thermal Engineering, 2016, 99, 1110-1118.
- [12] Z. Wang, H. Kuang, J. Zhang, L. Chu and Y. Ji, Nitrogen oxide removal by non-thermal plasma for marine diesel engines, RSC Advances, 2019, 9, 5402-5416.
- [13] M. Babaie, T. Kishi, M. Arai, Y. Zama, T. Furuhashi, Z. Ristovski, H. Rahimzadeh and R.J. Brown, Influence of non-thermal plasma after-treatment technology on diesel engine particulate matter composition and NO_x concentration, International Journal of Environmental Science and Technology, 2016, 13, 221-230.
- [14] M.R. Khani, E.B. Pour, S. Rashnoo, X. Tu, B. Ghobadian, B. Shokri, A. Khadem and S.I. Hosseini, Real diesel engine exhaust emission control: indirect non-thermal plasma and comparison to direct plasma for NO_x, THC, CO, and CO₂, Journal of Environmental Health Science and Engineering, 2020, 181, 743-754.
- [15] T. Wang, X. Zhang, J. Liu, H. Liu, Y. Wang and B. Sun, Effects of temperature on NO_x removal with Mn-Cu/ZSM5 catalysts assisted by plasma, Applied Thermal Engineering, 2018, 130, 1224-1232.
- [16] I. Jögi, K. Erme, J. Raud and E. Stamat, Plasma and catalyst for the oxidation of NO_x, Plasma Sources Science and Technology, 2018, 27, 035001.
- [17] P. Wang, W. Gu, L. Lei, Y. Cai, and Z. Li, Micro-structural and components evolution mechanism of particular matter from diesel engines with non-thermal plasma technology, Applied Thermal Engineering, 2015, 91(3), 1-10.
- [18] M. Rattanathom, S. Chuepeng and S. Gururatana, Physio-geometrical characterization of combustion generated nano-particle emissions from a palm oil based biodiesel fueled agricultural engine, The Journal of Industrial Technology, 2018, 14(1), 22-39.
- [19] C.S. Cheung, X.J. Man, K.W. Fong and O.K. Tsang, Effect of waste cooking oil biodiesel on the emissions of a diesel engine, Energy Procedia, 2015, 66, 93-96.



- [20] J. Bunker, J. Krahl, K. Baum, O. Schroder, M. Muller, G. Westphal, P. Ruhnau, T.G. Schulz and E. Hallier, Cytotoxic and mutagenic effects, particle size and concentration analysis of diesel engine emissions using biodiesel and petrol diesel as fuel, *Archives of Toxicology*, 2000, 74, 490-498.
- [21] X.J. Mana, C.S. Cheung, Z. Ning, L. Wei and Z.H. Huang, Influence of engine load and speed on regulated and unregulated emissions of a diesel engine fueled with diesel fuel blended with waste cooking oil biodiesel, *Fuel*, 2016, 180, 41-49.
- [22] L. Wei, C.S. Cheung and Z. Ning, Influence of waste cooking oil biodiesel on combustion, unregulated gaseous emissions and particulate emissions of a direct-injection diesel engine, *Energy*, 2017, 127, 175-185.
- [23] A.N. Ozsezen, M. Canakci, A. Turkcan and C. Sayin, Performance and combustion characteristics of a DI diesel engine fueled with waste palm oil and canola oil methyl esters, *Fuel*, 2009, 88(4), 629-636.
- [24] M.S. Koçak, E. Ileri and Z. Utlu, Experimental study of Emission parameters of biodiesel fuels obtained from canola, hazelnut, and waste cooking oils, *Energy & Fuels*, 2007, 21(6), 3622-3626.
- [25] R.G. Ewing and M.J. Waltman, Production and utilization of CO_3^- produced by a corona discharge in air for atmospheric pressure chemical ionization, *International Journal of Mass Spectrometry*, 2010, 296, 53-58.
- [26] J. Gao, C. Ma, S. Xing and L. Sun, Oxidation behaviours of particulate matter emitted by a diesel engine equipped with a NTP Device, *Applied Thermal Engineering*, 2017, 119, 593-602.
- [27] J. Gao, C. Ma, S. Xing, L. Sun and L. Huang, Nanostructure analysis of particulate matter emitted from a diesel engine equipped with a NTP reactor, *Fuel*, 2017, 192, 35-44.
- [28] Z. Bo, J. Yan, X. Li, Y. Chi and K. Cen, Nitrogen dioxide formation in the gliding arc discharge-assisted decomposition of volatile organic compounds, *Journal of Hazardous Materials*, 2009, 166, 1210-1216.
- [29] C. Song, F. Bin, Z. Tao, F. Li and Q.. Huang, "Simultaneous removals of NO_x , HC and PM from diesel exhaust emissions by dielectric barrier discharges, *Journal of Hazardous Materials*, 2009, 166, 523-530.
- [30] P. Rounce, A. Tsolakis and A.P.E. York, Speciation of particulate matter and hydrocarbon emissions from biodiesel combustion and its reduction by aftertreatment, *Fuel*, 2012, 96, 90-99.



- [31] B.M. Penetrante and S.E. Schultheis. Non-thermal plasma techniques for pollution control: Part B - Electron beam and electrical discharge processing, Springer Verlag, Berlin, 1993.
- [32] T. Wongchang, S. Sittichompoo, K. Theinnoi, B. Sawatmongkhon and S. Jugjai, Impact of high-voltage discharge after-treatment technology on diesel engine particulate matter composition and gaseous emissions, ACS Omega, 2021, 6(32), 21181-21192.
- [33] J. Jolibois, K. Takashima and A. Mizuno, Application of a non-thermal surface plasma discharge in wet condition for gas exhaust treatment: NO_x removal, Journal of Electrostatics, 2012, 70, 300-308.
- [34] P. Talebizadeh, M. Babaie, R. Brown, H. Rahimzadeh, Z. Ristovski and M. Arai, The role of non-thermal plasma technique in NO_x treatment: A review, Renewable and Sustainable Energy Reviews, 2014, 40, 886-901.
- [35] S. Thitipatanapong, S. Chuepeng and P. Visuwan, Characterization of particulate from biodiesel-blended engine equipped with exhaust nonthermal plasma charger using thermo-gravimetric analysis, SAE Technical Paper, 2015, 2015-01-0111.
- [36] J. Chae, Non-thermal plasma for diesel exhaust treatment, Journal of Electrostatics, 2003, 57, 251-262.
- [37] T. Kuroki, M. Ishidate, M. Okubo and T. Yamamoto, Charge-to-mass ratio and dendrite structure of diesel particulate matter charged by corona discharge, Carbon, 2010, 48, 184-190.
- [38] M. Okubo, N. Arita, T. Kuroki and T. Yamamoto, Total diesel emission control technology using ozone injection and plasma desorption, Plasma Chemistry and Plasma Processing, 2008, 28, 173-187.
- [39] M. Babaie, P. Davari, P. Talebizadeh, F. Zare, H. Rahimzadeh, Z. Ristovski and R. Brown, Performance evaluation of non-thermal plasma on particulate matter, ozone and CO₂ correlation for diesel exhaust emission reduction, Chemical Engineering Journal, 2015, 276, 240-248.